JOURNAL OF MAGNETIC RESONANCE, Series A 102, 195–204 (1993)

Sideband Patterns in Dynamic-Angle-Spinning NMR

P. J. GRANDINETTI, Y. K. LEE,* J. H. BALTISBERGER, B. Q. SUN, AND A. PINES

Materials Sciences Division, Lawrence Berkeley Laboratory, 1 Cyclotron Road, Berkeley, California 94720; and Department of Chemistry, University of California, Berkeley, California 94720

Received June 9, 1992; revised August 18, 1992

It is known that dynamic-angle-spinning (DAS) NMR can be accomplished using a variety of complementary angles (θ_1, θ_2) characterizing the two orientations of the spinner axis with respect to the magnetic field. In cases where the evolution period of the two-dimensional DAS experiment is divided into unequal parts, for example, by RF pulses or spinner reorientation, a complex sideband pattern emerges. We describe a simple theory of the sideband pattern and provide illustrative experimental results of spectra over a range of DAS angles. The DAS experiment with the angle pair (0°, 63.43°) has sidebands at integer multiples of $0.83\Omega_R$ and should be particularly useful for DAS cross-polarization experiments involving central transitions of quadrupolar nuclei. Our considerations are relevant to other NMR experiments in which an evolution time is composed of periods separated by a perturbation and/or characterized by different effective Hamiltonians.

INTRODUCTION

Spinning sidebands appear in a nuclear magnetic resonance spectrum when the Hamiltonian describing the system has a periodic time dependence and a rotational frequency greater than the homogeneous linewidth of the system. This situation commonly occurs in rotating liquids in an inhomogeneous magnetic field (*1*) or in a rotating solid with an anisotropic Hamiltonian (*2–6*). Spinning sidebands usually appear at integral multiples of the rotation frequency with the intensity decreasing with increasing integer multiple and increasing rotation frequency. However, in certain types of two-dimensional NMR experiments, in particular, 2D echo spectroscopy, spinning sidebands can exhibit a much more complex behavior. An example of this behavior was observed by Bodenhausen *et al.* (*7*) in 2D *J* spectroscopy in which the spinning sidebands appeared at multiples of half the spinning frequency in the ω_1 dimension. This behavior is the result of the two equal periods of evolution separated by the echo π pulse. Kolbert *et al.* (*8*) later utilized this behavior in a 2D solid-state NMR spin-echo experiment to correlate the anisotropic information available from the sideband intensities of an effectively slower spinning sample in the first dimension with the simpler relatively sideband-free spectrum in the second dimension. They also showed how additional π pulses can be employed in t_1 with a corresponding increase in the number of sidebands.

The recently developed technique of dynamic-angle spinning (DAS) (*9–11*) naturally involves a 2D echo experiment, the two periods of evolution being defined by the two DAS spinning angles (θ_1, θ_2). Because the refocusing time is not necessarily equal to the dephasing time, DAS can display a more complex spinning-sideband pattern. In addition, the amplitudes of the DAS spinning sidebands vary as the magnitude of the time-dependent components of the Hamiltonian change during the refocusing and dephasing times under different spinning-axis angles. In this paper we provide a general approach that explains the patterns of spinning sidebands in DAS and related NMR experiments involving partitioned evolution periods. Our treatment provides a simple intuitive description that complements previous theories of 2D echo experiments (*7, 8*).

Spinning sidebands spaced at noninteger multiples of the actual spinning speed can be obtained in the isotropic dimension of a DAS experiment. By proper choice of the complementary angle pair (θ_1, θ_2) in a DAS experiment designed to remove second-order broadenings, spinning sidebands spaced at 0.83 times the actual spinning speed can be obtained in the isotropic dimension, an increase over the value of 0.5 previously reported for DAS (*11*). In addition, we describe how sidebands spaced at 1.33 times the actual spinning speed can be obtained in the isotropic dimension of a DAS experiment designed to remove only first-order broadenings.

EXPERIMENTAL

All spectra were taken in an 11.7 T magnet using a home-built DAS probe (*12*). A modified version of the DAS experiment (*13*) that provides pure-absorption-phase spectra was employed and all experiments were obtained without synchronization of the rotor. The evolution times at each

* Health Effects Research Division, Lawrence Berkeley Laboratory, 1 Cyclotron Road, Berkeley, California 94720; and Biophysics Group, University of California, Berkeley, California 94720.

1064-1858/93 $5.00

rotor angle in the DAS experiments were separated by a constant spinner-axis reorientation delay of approximately 30 ms. $RbClO_4$ and $PbNO_3$ were obtained from Aldrich and used without further purification.

THEORY

We consider the case of a periodic time-dependent Hamiltonian, $\mathscr{H}(t)$, with adiabatic behavior under sample rotation about a single axis at a frequency Ω_R. The arguments presented here can also be applied to more complex time dependences such as that characteristic of double rotation (*14*).

The unperturbed evolution operator, $U(t, 0)$, obtained from $\mathscr{H}(t)$ through the Schrödinger equation,

$$i\dot{U}(t, 0) = \mathscr{H}(t)U(t, 0), \qquad [1]$$

contains frequency components characteristic of $\mathscr{H}(t)$, which in the case of sample rotation includes frequency components separated by integer multiples of Ω_R. In contrast, when perturbations, R, are applied during the evolution time, the perturbed evolution operator,

$$U(t, 0) = U(t, t - x_{n-1}t)R_{n-1} \cdots R_2U(x_2t + x_1t, x_1t)R_1U(x_1t, 0), \qquad [2]$$

can contain frequency components that differ significantly from the unperturbed evolution operator and in the case of sample rotation, can include frequency components separated by noninteger multiples of Ω_R. Here, the parameters x_j are constrained such that $\sum_j^n x_j = 1$, and the perturbations R may take the form of RF pulses, rotor reorientations, gradient switching, etc. The basic premise is that through a transformation of time variables, which may require an increase in dimensionality, any perturbed NMR experiment can be redefined in terms of unperturbed evolution times where the frequency components in each associated time evolution operator are easily predicted and can be related to the frequency components in the original experiment through a similarity transform or a skew projection.

Consider, for example, the pulse sequences shown in Fig. 1. Although the perturbations R_0 and R_1 are identical in both sequences, the resonance frequencies in either 2D spectrum can differ significantly due to the different definition of time variables. This difference between the resonance frequencies of the two experiments can be explained in terms of a similarity transform. It is well known (*15*) that a transformation of the variables in one domain is reflected by a corresponding transformation in the other (Fourier transform) domain. Using the notation of Ref. (*15*) the transformation of time variables between the pulse sequences in Fig. 1, given by

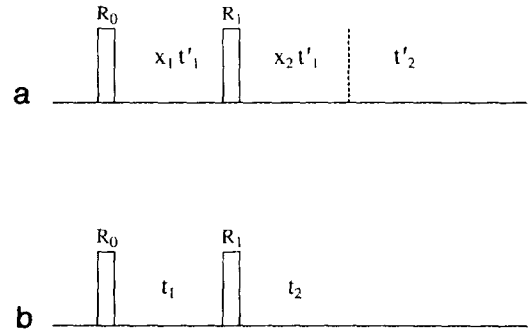

FIG. 1. Two identical pulse sequences with different time-variable definitions. The data acquired with these two sequences are related by a shearing transformation.

$$\mathbf{t}' = \mathscr{A}\mathbf{t}, \quad \text{where } s'(\mathbf{t}) = s(\mathscr{A}\mathbf{t}), \qquad [3]$$

and

$$\mathscr{A} = \begin{bmatrix} 1/x_1 & 0 \\ -x_2/x_1 & 1 \end{bmatrix}, \qquad [4]$$

corresponds to a transformation of the frequency variables given by

$$\tilde{\omega} = \tilde{\omega}.\mathscr{A}^{-1}, \quad \text{where } S'(\tilde{\omega}) = \frac{1}{|\mathscr{A}|} S(\tilde{\omega}.\mathscr{A}^{-1}), \qquad [5]$$

and

$$\mathscr{A}^{-1} = \begin{bmatrix} x_1 & 0 \\ x_2 & 1 \end{bmatrix}. \qquad [6]$$

This transformation is accomplished by a "shearing" of the frequency-domain data from the sequence in Fig. 1b with an angle, θ_s, given by

$$\theta_s = \tan^{-1}\frac{x_2}{x_1}, \qquad [7]$$

followed by a scaling of the ω_1 axis by x_1. Shearing transformations are well known in two-dimensional NMR (*16–20*) and as we shall show provide a simple picture for understanding sideband patterns in DAS.

A schematic example of the behavior of spinning sidebands after a shearing transformation is shown in Fig. 2 for two cases where $\theta_s = 45°$ and $\theta_s = 38.7°$. The frequency axes in Fig. 2a are in units of Ω_R, the actual spinning speed. The example in Fig. 2b is the familiar situation in 2D echo spectroscopy, where the dephasing and refocusing times are equal (e.g., 2D J spectroscopy). In this example even though the

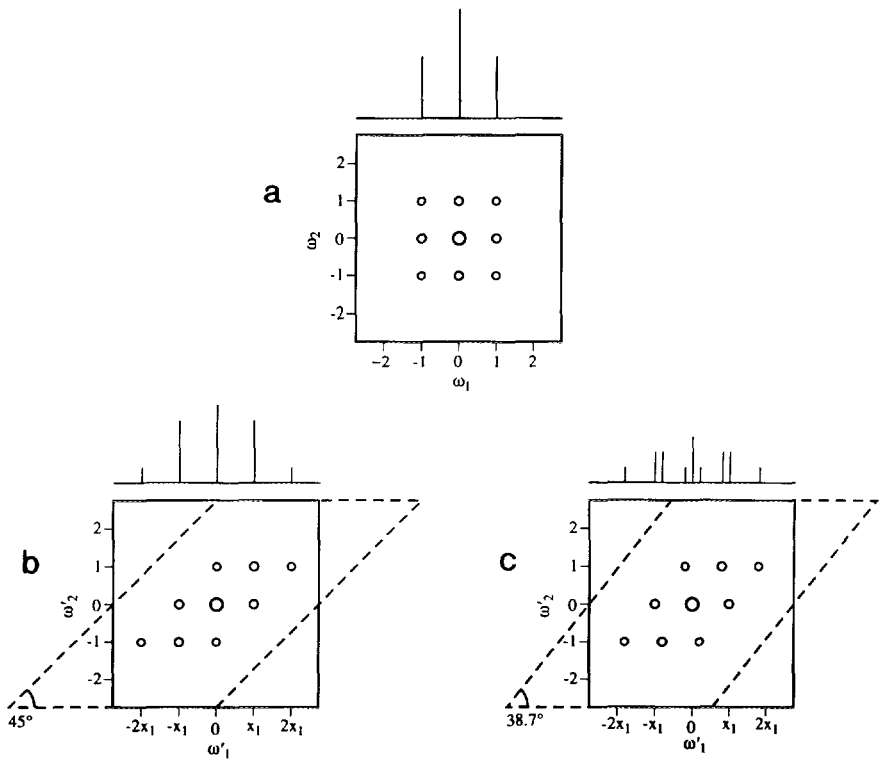

FIG. 2. Schematic examples of the shearing transformation relating the two-dimensional spectra obtained from the two pulse sequences in Fig. 1. (a) Two-dimensional spectrum obtained using pulse sequence in Fig. 1b. (b) Two-dimensional spectrum obtained using the pulse sequence in Fig. 1a. This case corresponds to equal dephasing and refocusing times ($x_1 = x_2 = 0.5$) and is obtained from the two-dimensional spectrum in a by a shearing transformation that employs a shearing angle of 45° and a scaling of the ω_1 by $x_1 = 0.5$. In this case the spinning sidebands in the two-dimensional spectrum are aligned with respect to ω'_1 so that a projection onto the ω'_1 axis contains only spinning sidebands separated by integer multiples of $0.5\Omega_R$. (c) Two-dimensional spectrum obtained using the pulse sequence in Fig. 1a. This case corresponds to unequal dephasing and refocusing times ($x_1 = 0.56$ and $x_2 = 0.44$) and is obtained from the original two-dimensional spectrum in a by a shearing transformation employing a shearing angle of 38.7° and a scaling of the ω_1 by $x_1 = 0.56$. In this case the spinning sidebands in the two-dimensional spectrum are not aligned with respect to ω'_1 so that a projection onto the ω'_1 axis contains spinning sidebands that are separated by multiples of and also sum and difference frequencies of $x_1\Omega_R = 0.56\Omega_R$ and $x_2\Omega_R = 0.44\Omega_R$.

spectrum is sheared, the sidebands remain aligned such that a projection onto the ω'_1 axis contains only sidebands at integer multiples of $0.5\Omega_R$. In contrast, the example in Fig. 2c, where $x_1 = 0.44$ and $x_2 = 0.56$, describes a 2D echo experiment with unequal dephasing and refocusing times. In this situation the spinning sidebands are not aligned in ω'_1, and consequently a projection onto ω'_1 yields a fairly complicated sideband pattern. In the next section we present examples of such DAS experiments that use unequal dephasing and refocusing times and the associated complicated sideband behavior.

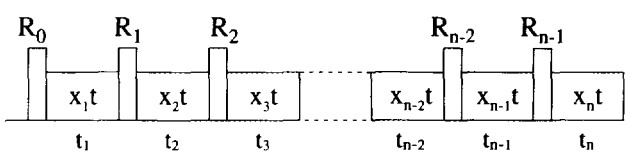

FIG. 3. Redefinition of a one-dimensional perturbed evolution period, t, into multidimensional unperturbed evolution periods, $t_1, t_2, \ldots, t_n$.

In general, for an arbitrary number of perturbations during the evolution time, the perturbed evolution time can be redefined in terms of smaller unperturbed evolution times, as in Fig. 3, with an increase in the dimensionality of the experiment, where

$$U(t_1, \ldots, t_n) = U(T, T - t_n)R_{n-1} \cdots R_2U(t_2 + t_1, t_1)R_1U(t_1, 0), \quad [8]$$

and $T = \sum_j^n t_j$. Upon Fourier transformation of this n-dimensional experiment, the spinning sidebands will appear at integer multiples of Ω_R in every dimension. A projection of this n-dimensional spectrum onto an axis given by the direction cosines l_i, where

$$l_i = \frac{x_i}{\sqrt{\sum_j x_j^2}}, \quad [9]$$

followed by a rescaling of the projection axis by $\sqrt{\sum_j x_j^2}$ pro-

vides the frequency-domain spectrum of the one-dimensional perturbed evolution under the operator in Eq. [2]. Spinning sidebands separated by Ω_R in the unperturbed dimension ω_j will then be separated by $x_j\Omega_R$ on the projected axis. This procedure is similar to accordian spectroscopy (*21*), where a concerted variation of two evolution times (t_1 and τ_m) reduces a three-dimensional experiment to a two-dimensional experiment.

Although the simple arguments of similarity transformations or projections describe the frequency positions of the spinning sidebands under perturbed evolutions, details of the sideband amplitudes will depend on the specifics of the perturbations. To illustrate this we consider a DAS experiment on the central transition of a half-integer quadrupolar nucleus. To second order, the central transition frequency in the rotating frame may be expanded as (see Appendix)

$$\Omega^{(2)}(\theta, t) = \sum_{n=-4}^{4} W_n(\beta, \gamma, \theta)e^{in(\Omega_R t+\alpha)}, \qquad [10]$$

where Ω_R is the rotor frequency, α, β, and γ are the Euler angles between the principal-axis system of the quadrupolar interaction and the rotor-axis system, and θ is the angle of the rotor spinning axis with respect to the external magnetic field. In the simplest implementation of DAS, R_0 is a $\pi/2$ pulse, and R_1 is a perturbation that is composed of two $\pi/2$ pulses separated by a constant length of time during which the rotor axis is switched. The signal in terms of the unperturbed evolution times t_1 and t_2 can be written

$$S(t_1, t_2) = e^{iW_0(\beta,\gamma,\theta_1)t_1}e^{iW_0(\beta,\gamma,\theta_2)t_2} \times \sum_{N_1=-\infty}^{\infty}\sum_{N_2=-\infty}^{\infty}\sum_{N_3=-\infty}^{\infty}\sum_{N_4=-\infty}^{\infty} A_{N_1}(\theta_1)A^*_{N_2}(\theta_1)A_{N_3}(\theta_2)A^*_{N_4}(\theta_2) \times e^{-i[(N_1-N_2+N_3-N_4)\alpha+(N_1+N_3-N_4)\Omega_R t_1+N_3\Omega_R t_2+(N_3-N_4)\phi_R]}, \qquad [11]$$

where ϕ_R is the constant rotor phase accumulated during the hop, and the $A_N(\theta)$ are given the Appendix. The unsheared 2D DAS spectrum can thus be written as a product of the one-dimensional variable-angle-spinning (VAS) spectra associated with each rotor angle. In general, a correlation between two VAS spectra will depend parametrically on the powder angles β and γ. However, for the special DAS complementary rotor-angle pairs for which

$$x_1 W_0(\beta, \gamma, \theta_1) = -x_2 W_0(\beta, \gamma, \theta_2), \qquad [12]$$

the correlation between associated VAS spectra will be a linear isotropic correlation. There exists a continuous set of angle pairs, (θ_1, θ_2), that satisfies Eq. [12]. A similarity transformation of this correlated 2D VAS experiment, implemented by a shear of angle $\tan^{-1}x_2/x_1$ followed by a scaling of the ω_1 axis by x_1, results in the 2D DAS spectrum.

It is easily proved that the centerband and sideband amplitudes in the projection onto the ω_1 or ω_2 axis of the correlated 2D VAS spectrum are all real and positive (*22*). Experimentally, we have observed that all sidebands and centerbands in the 2D DAS spectrum are also real and positive. In general, this may not be true for all sidebands in a 2D DAS spectrum; however, numerical simulations of 2D DAS spectra confirm our experimental observations that all sidebands of significant intensity do indeed have the same phase. In the Appendix we analytically show that if specific rotor angles are used, or if averages over certain experimental variables are taken, the sidebands in the 2D DAS spectrum will be real and positive. Therefore, for the remaining discussion we assume, in general, that all sidebands and centerbands in the 2D DAS spectrum have the same phase. Thus, knowledge of the sideband amplitudes and positions for the 1D VAS spectrum associated with each DAS angle can aid in predicting the sideband amplitudes and positions in any 2D DAS spectrum. In the next section we use this approach to explain the sideband patterns that can be observed in DAS experiments.

RESULTS AND DISCUSSION

In many 2D echo NMR experiments the dephasing and refocusing times are equal (i.e., $x_1 = 0.5$ and $x_2 = 0.5$), and the spinning sidebands appear at multiples of $0.5\Omega_R$ in ω'_1. In the DAS experiment the dephasing and refocusing times are not necessarily equal, and the values of x_1 and x_2 will depend on the rotor-angle pair used. When first- and second-order anisotropic broadenings are removed with DAS, equal dephasing and refocusing times are obtained with the rotor angle pair $\theta_1 = 37.38°$ and $\theta_2 = 79.19°$, and, as noted previously (*11*), when using this angle pair, spinning sidebands are obtained at multiples of $0.5\Omega_R$ in the isotropic DAS dimension. A 2D ^{87}Rb NMR spectrum of $RbClO_4$ correlating the 37.38° and 79.19° VAS spectra is shown on the left in Fig. 4. Spinning sidebands appear at multiples of Ω_R in both dimensions. The correlated 2D (37.38°, 79.19°) VAS spectrum can be transformed into a 2D DAS spectrum using a shearing of 45° followed by a scaling of ω_1 by 0.5, the same transformation used in the schematic example of Fig. 2, whereby the spectrum in Fig. 2b was obtained from that in Fig. 2a. Thus all the sidebands are aligned in ω'_1 and a projection onto the ω'_1 axis provides an isotropic DAS spectrum with spinning sidebands equally spaced at multiples of $0.5\Omega_R$. The projection onto the ω'_2 axis provides the VAS spectrum characteristic of the final rotor angle, in this case 79.19°.

The situation for unequal dephasing and refocusing times is illustrated by the 2D DAS ^{87}Rb NMR spectrum of $RbClO_4$ in Fig. 5, in which the DAS angle pair $\theta_1 = 39.23°$ and $\theta_2 = 90°$ was used, corresponding to $x_1 = 0.44$ and $x_2 = 0.56$. Using the same shearing transformation applied in the schematic example of Fig. 2c, the 2D DAS spectrum in Fig. 5

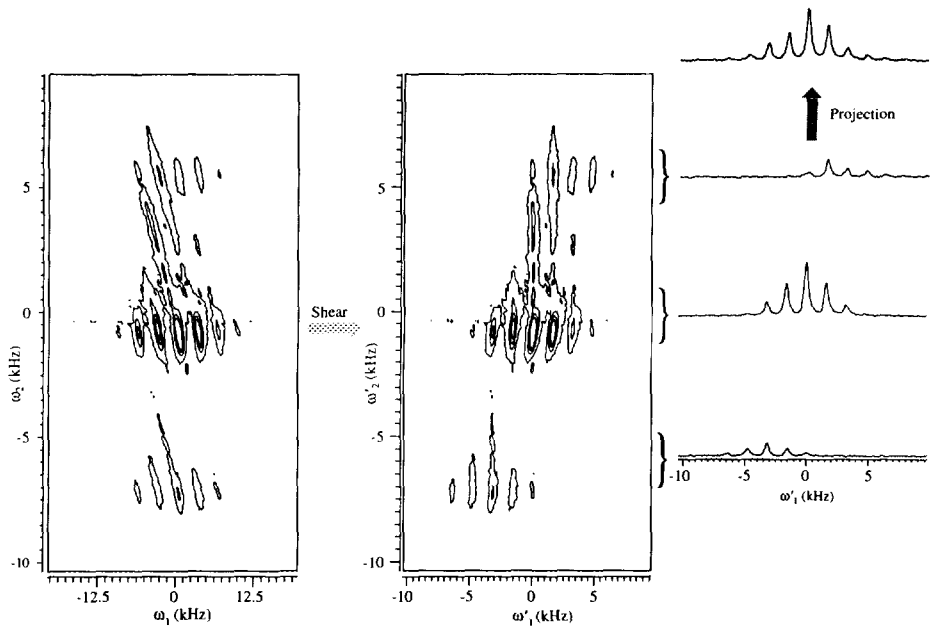

FIG. 4. On the left is a $^{87}RbClO_4$ 2D NMR spectrum correlating the VAS spectra of the DAS angle pair $\theta_1 = 37.38°$ and $\theta_2 = 79.19°$. This 2D VAS-correlated spectrum is transformed into the 2D DAS spectrum on the right using a shearing transformation as described in the text and in the legend to Fig. 2 when $x_1 = x_2 = 0.5$. The rotor frequency was $\Omega_R = 3.2$ kHz. In this example the spinning sidebands in the 2D DAS spectrum are aligned with respect to ω'_1 so that a projection onto the ω'_1 axis contains only spinning sidebands separated by integer multiples of $0.5\Omega_R = 1.6$ kHz.

was obtained from the correlated 2D (39.23°, 90°) VAS spectrum. In this example the spinning sidebands are not aligned in ω'_1. So even though each of the ω'_2 slices in Fig. 5 resembles the ω'_2 slices in Fig. 4 the overall projection on to the ω'_1 axis in Fig. 5 yields a much more complicated sideband pattern in the isotropic DAS dimension.

Simulated isotropic projections from the ^{87}Rb DAS of $RbClO_4$, demonstrating the sideband behavior for various different pairs of DAS angles, are shown in Fig. 6. In each isotropic 1D DAS spectrum the spinning sidebands appear at integer multiples of $x_1\Omega_R$ and $x_2\Omega_R$ and also at the sum and difference frequencies of integer multiples of $x_1\Omega_R$ and $x_2\Omega_R$. The angle pair (37.78°, 79.19°) has an advantage that $x_1\Omega_R = x_2\Omega_R = 0.5\Omega_R$ and a simple sideband spacing of $0.5\Omega_R$ is obtained. Of particular interest is the fact that the 1D DAS spectrum for the (0°, 63.43°) angle pair contains only spinning sidebands at multiples of $x_2\Omega_R = 0.83\Omega_R$. The spinning sidebands at $x_1\Omega_R = 0.17\Omega_R$ do not exist, and thus the (0°, 63.43°) angle pair provides the highest effective spinning speed when removing first- and second-order broadenings with DAS. The experimental isotropic DAS projections are shown in Fig. 7 and indeed bear out these expectations.

The particular simplification of the sideband spectrum for the (0°, 63.43°) angle pair is due to the fact that all time-dependent terms have zero amplitudes when the sample is rotating about 0°. Thus the sideband behavior for the (0°, 63.43°) DAS experiment can be easily understood when one considers the correlated 2D (0°, 63.43°) VAS spectrum shown on the left in Fig. 8. While the 63.43° VAS spectrum contains spinning sidebands at integer multiples of Ω_R, the 0° VAS spectrum contains no sidebands. The 2D DAS spectrum on the right in Fig. 4 is obtained after a shearing transformation employing a shearing angle of 78.69° and a scaling of the ω_1 axis by 0.17. The projection of this 2D DAS spectrum onto the ω'_1 axis contains only spinning sidebands at integer multiples of $0.83\Omega_R$.

In the case of first-order broadenings, it is possible to increase the effective spinning speed in the isotropic dimension beyond the actual spinning speed using the arguments above. By combining the fact that the 0° VAS spectrum contains no spinning sidebands with the fact that the 90° VAS spectrum contains only spinning sidebands at multiples of $2\Omega_R$, we can design a DAS experiment that removes only first-order broadenings with spinning sidebands occuring only at multiples of $1.33\Omega_R$ in the isotropic dimension. For first-order broadenings the (0°, 90°) angle pair satisfies Eq. [12], with $x_1 = 0.33$ and $x_2 = 0.67$. In Fig. 9 is the 2D DAS ^{207}Pb NMR spectrum of $PbNO_3$ using the $\theta_1 = 0°$ and $\theta_2 = 90°$ angle pair. Since there are no spinning sidebands in the 0° VAS spectrum the spinning sidebands in the isotropic DAS dimension at integer multiples of $x_1\Omega_R$ do not exist. In the 90° VAS spectrum, only spinning sidebands at integer multiples of $2\Omega_R$ exist, and so, after the shearing transformation of the 2D (0°, 90°) VAS spectrum, these spinning sidebands are projected onto the isotropic DAS dimension at integer multiples of $x_2 2\Omega_R = 1.33\Omega_R$.

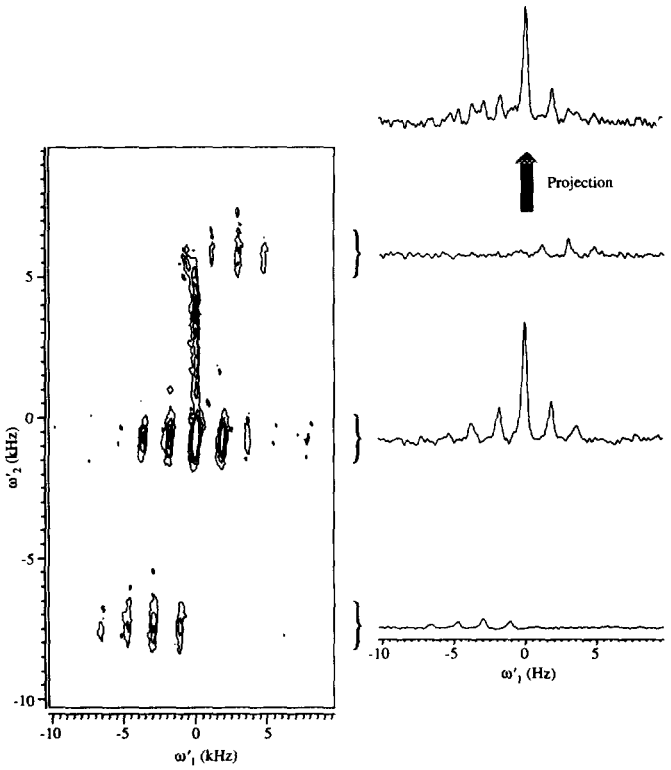

FIG. 5. Two-dimensional DAS spectrum of $^{87}RbClO_4$ using $\theta_1 = 39.23°$ and $\theta_2 = 90°$, where $x_1 = 0.56$ and $x_2 = 0.44$. The rotor frequency was $\Omega_R = 3.2$ kHz. In this example the spinning sidebands in the 2D DAS spectrum are not aligned with respect to ω'_1 and a projection onto the ω'_1 axis contains spinning sidebands separated by multiples of and also sum and difference frequencies of $0.56\Omega_R = 1.8$ kHz and $0.44\Omega_R = 1.4$ kHz.

An important aspect of the sideband simplifications described above is that the intensities of the suppressed sidebands in the isotropic dimension are transferred to the centerband and other sidebands. This is easily seen by noting that the integrated intensity of the 2D DAS spectrum must be constant regardless of which rotor-angle pair is used. Thus, for example, the intensities of the $x_1\Omega_R$ spinning sidebands in the (0°, 63.43°) DAS experiment are not lost, but have been transferred to the centerband and the $x_2\Omega_R$ spinning sidebands. This is in contrast to other sideband manipulation techniques like TOSS or PASS (*23*), where the intensities of suppressed sidebands are not necessarily transferred to the centerband. This can be seen using the approach outlined in the previous section to analyze the simple two-pulse TOSS sequence for eliminating first-order sidebands (*24*). The propagator for this experiment can be written as a three-dimensional experiment with unperturbed evolution periods t_1, t_2, and t_3, where

$$U(t_3, t_2, t_1) = U(t_3 + t_2 + t_1, t_2 + t_1) \times R_2U(t_2 + t_1, t_1)R_1U(t_1, 0), \quad [13]$$

and R_1 and R_2 are π pulses. This three-dimensional experiment correlates the MAS spectrum with itself and contains spinning sidebands appearing at integer multiples of Ω_R in all dimensions. The one-dimensional TOSS spectrum is then obtained from this three-dimensional time-domain data by a cross section taken parallel to the t_3 axis, intercepting the t_2 and t_1 axes at the constant times τ_2 and τ_1 and starting at a constant time delay τ_3. The constant times τ_i are the calculated fractions of the rotor period needed to cancel the first-order spinning sidebands. In the frequency domain, this cross section corresponds to a projection onto the ω_3 axis after linear phase corrections given by

$$\phi_i(\omega_i) = \omega_i\tau_i \quad [14]$$

have been applied to each ω_i dimension. These phase corrections have the effect of modulating the spinning-sideband amplitudes in the three-dimensional spectrum so that, in the final projection onto the ω_3 axis, the first-order sidebands cancel. In general, with TOSS the spinning sidebands at all multiples of Ω_R are present in the multidimensional spectrum and vanish only in the projection onto the final axis. In con-

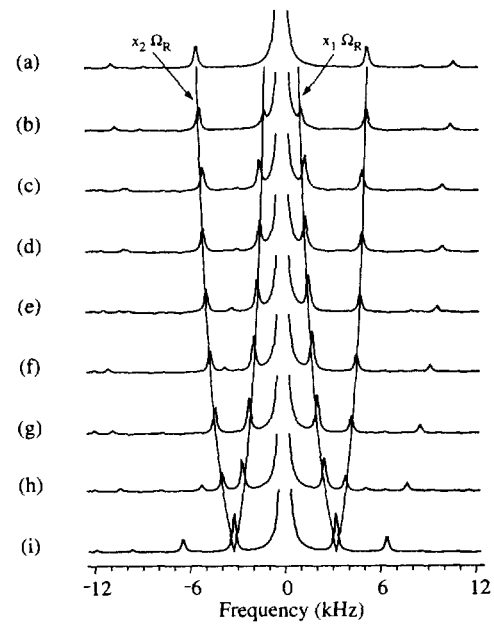

FIG. 6. Simulated 1D DAS spectra of $^{87}RbClO_4$ for various rotor-angle pairs (θ_1, θ_2). (a) $\theta_1 = 0°$ and $\theta_2 = 63.43°$, where $x_1 = 0.17$ and $x_2 = 0.83$, (b) $\theta_1 = 10.66°$ and $\theta_2 = 63.96°$, where $x_1 = 0.18$ and $x_2 = 0.82$, (c) $\theta_1 = 15.38°$ and $\theta_2 = 64.58°$, where $x_1 = 0.2$ and $x_2 = 0.80$, (d) $\theta_1 = 19.27°$ and $\theta_2 = 65.35°$, where $x_1 = 0.22$ and $x_2 = 0.78$, (e) $\theta_1 = 22.81°$ and $\theta_2 = 66.33°$, where $x_1 = 0.25$ and $x_2 = 0.75$, (f) $\theta_1 = 26.22°$ and $\theta_2 = 67.64°$, where $x_1 = 0.29$ and $x_2 = 0.71$, (g) $\theta_1 = 29.67°$ and $\theta_2 = 69.51°$, where $x_1 = 0.33$ and $x_2 = 0.67$, (h) $\theta_1 = 33.31°$ and $\theta_2 = 72.55°$, where $x_1 = 0.4$ and $x_2 = 0.6$, (i) $\theta_1 = 37.38°$ and $\theta_2 = 79.19°$, where $x_1 = 0.5$ and $x_2 = 0.5$. All spectra were obtained with a rotor frequency of $\Omega_R = 6.4$ kHz. The quadrupolar coupling parameters of $RbClO_4$ used in the simulations are $C_q = 3.2$ MHz and $\eta = 0.1$.

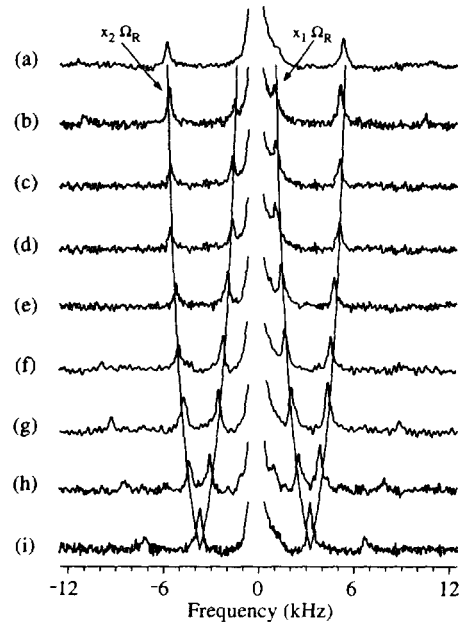

FIG. 7. Experimental 1D DAS spectra of $^{87}RbClO_4$ for various rotor-angle pairs (θ_1, θ_2). (a) $\theta_1 = 0°$ and $\theta_2 = 63.43°$, where $x_1 = 0.17$ and $x_2 = 0.83$, (b) $\theta_1 = 10.66°$ and $\theta_2 = 63.96°$, where $x_1 = 0.18$ and $x_2 = 0.82$, (c) $\theta_1 = 15.38°$ and $\theta_2 = 64.58°$, where $x_1 = 0.2$ and $x_2 = 0.80$, (d) $\theta_1 = 19.27°$ and $\theta_2 = 65.35°$, where $x_1 = 0.22$ and $x_2 = 0.78$, (e) $\theta_1 = 22.81°$ and $\theta_2 = 66.33°$, where $x_1 = 0.25$ and $x_2 = 0.75$, (f) $\theta_1 = 26.22°$ and $\theta_2 = 67.64°$, where $x_1 = 0.29$ and $x_2 = 0.71$, (g) $\theta_1 = 29.67°$ and $\theta_2 = 69.51°$, where $x_1 = 0.33$ and $x_2 = 0.67$, (h) $\theta_1 = 33.31°$ and $\theta_2 = 72.55°$, where $x_1 = 0.4$ and $x_2 = 0.6$, (i) $\theta_1 = 37.38°$ and $\theta_2 = 79.19°$, where $x_1 = 0.5$ and $x_2 = 0.5$. All spectra were obtained with a rotor frequency of $\Omega_R = 6.4$ kHz.

trast, with DAS the spinning sidebands are already absent in the multidimensional spectrum, and thus there is no cancelling of sidebands or loss of sideband intensity in the projection onto any axis.

CONCLUSIONS

We have attempted to present a general approach for treating spinning sidebands in perturbed NMR experiments and have used this approach to describe the complex spinning-sideband behavior that is obtained in dynamic-angle-spinning experiments. We exploit the fact that through a transformation of time variables, which may require an increase in dimensionality, the experiment can be redefined in terms of unperturbed evolution times where the frequency components associated with the time evolution operator due to sample motion are easily understood. The redefined experiment can be related back to the original experiment through a similarity transform or a skew projection.

We have shown that the unsheared 2D DAS spectrum is a simple correlation between two variable-angle-spinning spectra, and that knowledge of the sideband amplitudes and positions in the one-dimensional VAS spectrum associated with each of the DAS angles reveals the sideband amplitudes and positions in the 2D DAS spectrum. Using this approach we have demonstrated that, in general, the spinning sidebands in the isotropic DAS dimension appear at multiples and sum and difference frequencies of $x_1\Omega_R$ and $x_2\Omega_R$, where x_1 and x_2 are the fractional dephasing and refocusing times in the total evolution time. The highest effective spinning speed when removing first- and second-order broadenings with DAS is 0.83 times the actual spinning speed and is obtained with the DAS angle pair (0°, 63.43°). We demonstrate how the effective spinning speed in the isotropic dimension can be extended to 1.33 times the actual spinning speed in a (0°, 90°) DAS experiment designed to remove only first-order broadenings such as chemical-shift anisotropy. Finally, we show that in these experiments which increase the effective spinning speed, the sideband intensity is completely transferred to the centerband and other sidebands without loss of any sideband intensity.

Of course, spinning-sideband behavior analogous to that observed in DAS should appear in the NMR of a liquid sample spinning in a static field gradient whose magnitude and direction are switched during an evolution period.

APPENDIX: CALCULATION OF THE DAS SIGNAL

Considering the central transition ($\frac{1}{2} \leftrightarrow -\frac{1}{2}$) of a quadrupolar nucleus as an isolated two-level system, the quadrupolar Hamiltonian truncated to second order (*25*) is given by the effective Hamiltonian

$$\mathcal{H}^{(2)} = -\Omega^{(2)} I_Z, \qquad [15]$$

where

$$\Omega^{(2)} = \frac{2[I(I+1) - \frac{3}{4}]}{\omega_Z} \sum_{m>0} \frac{R_{2m} R_{2-m}}{m}. \qquad [16]$$

The R_{2m} are the lattice parts of the quadrupolar Hamiltonian and depend on the orientation in the laboratory frame of the principal axis of the quadrupolar interaction. $R_{2m}R_{2-m}$ can be expanded as

$$R_{2m}R_{2-m} = \sum_{k,k'} \sum_{J=0,2,4} \langle J\,0|2\,2\,m\,-m\rangle \langle J\,k{+}k'|2\,2\,k\,k'\rangle \times \mathcal{D}^{(J)}_{k+k'0}(\alpha, \beta, \gamma)\rho_{2k}\rho_{2k'}, \qquad [17]$$

where $\mathcal{D}^{(J)}_{k+k'0}(\alpha, \beta, \gamma)$ is a Wigner rotation matrix element, $\langle J\,0|2\,2\,m\,-m\rangle$ and $\langle J\,k{+}k'|2\,2\,k\,k'\rangle$ are the Clebsch–Gordon coefficient $\langle J\,M|j_1\,j_2\,m_1\,m_2\rangle$, and

$$\rho_{20} = \frac{\sqrt{62}\pi C_q}{4I(2I-1)} = \frac{\omega_Q}{\sqrt{6}},$$

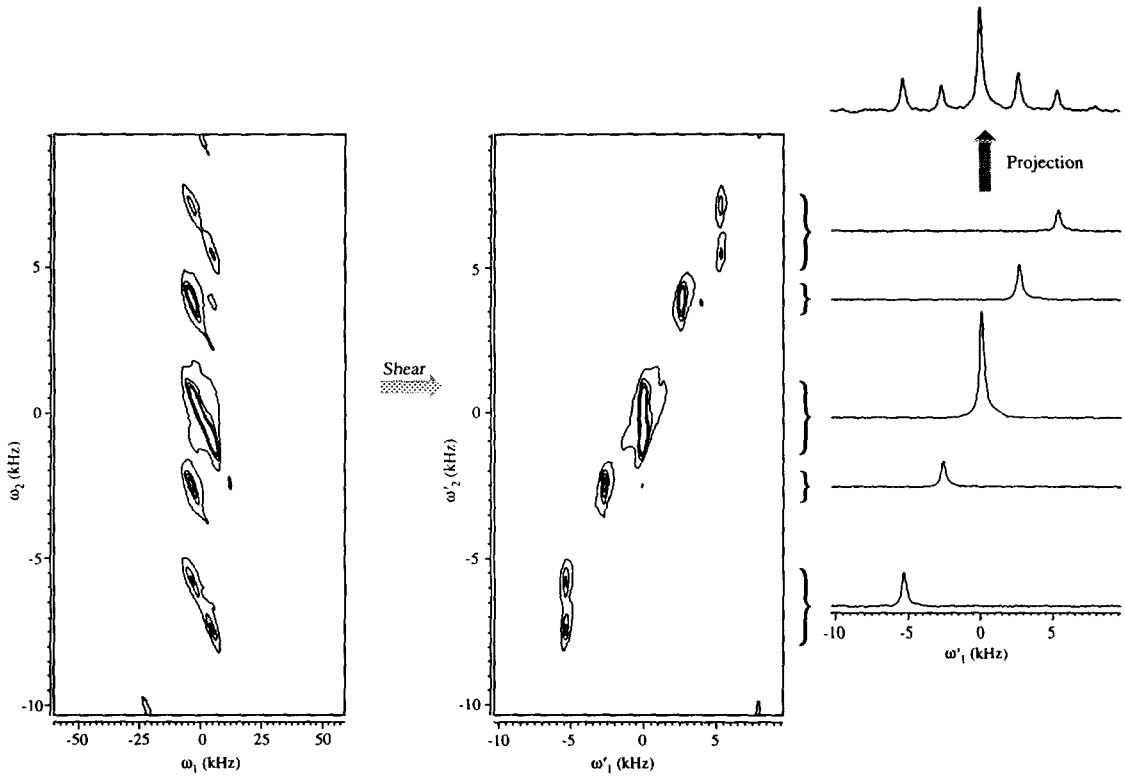

FIG. 8. On the left is a $^{87}RbClO_4$ 2D NMR spectrum correlating the VAS spectra of the DAS angle pair $\theta_1 = 0°$ and $\theta_2 = 63.43°$. The rotor frequency was $\Omega_R = 3.2$ kHz. Because the eigenvalues of the Hamiltonian when spinning at 0° are time independent, there are no spinning sidebands in a 0° VAS spectrum. Therefore only spinning sidebands associated with spinning at 63.43° will be present in the 2D (0°, 63.43°) VAS-correlated spectrum of a polycrystalline sample. After transforming this 2D VAS-correlated spectrum into the 2D DAS spectrum on the right using a shearing transformation as described in the text and in the legend to Fig. 2 ($x_1 = 0.17$ and $x_2 = 0.83$), a projection of the 2D DAS spectrum onto the ω'_1 axis contains only spinning sidebands separated by multiples of $0.83\Omega_R = 2.7$ kHz. Thus, the (0°, 63.43°) angle pair provides the highest effective spinning speed when first- and second-order broadenings are removed with DAS.

where

$$\rho_{2\pm1} = 0,$$

$$\rho_{2\pm2} = \frac{2\pi\eta C_q}{4I(2I-1)} = \frac{\eta\omega_Q}{6}, \qquad [18]$$

where

$$C_q = e^2qQ/h, \quad \omega_Q = \frac{6\pi C_q}{2I(2I-1)}. \qquad [19]$$

The Wigner rotation matrix in Eq. [17] may now be expanded in terms of two separate rotations. The first rotation is from the principal-axis system of the quadrupolar interaction through the Euler angles α, β, γ to the frame of the rotor. The second rotation is from the frame of the rotor, which is spinning at a frequency Ω_R about the angle θ, to the laboratory frame. We then obtain for the central transition frequency

$$\Omega^{(2)}(\theta, t) = \sum_{n=-4}^{4} W_n(\beta, \gamma, \theta)e^{in(\Omega_R t+\alpha)}, \qquad [20]$$

where

$$W_n(\beta, \gamma, \theta) = \Omega^{(2)}_{iso}\delta_{n0} + \Omega^{(2)}_n(\beta, \gamma, \theta), \qquad [21]$$

$$\Omega^{(2)}_{iso} = -\frac{[I(I+1) - \frac{3}{4}]}{5\omega_Z}\sum_k (-1)^k\rho_{2k}\rho_{2-k}, \qquad [22]$$

and

$$\Omega^{(2)}_n(\beta, \gamma, \theta) = \frac{2[I(I+1) - \frac{3}{4}]}{\omega_Z} \times \sum_{k,k'}\sum_{m>0}\sum_{J=2,4;J\leq|n|} \langle J\,0|2\,2\,m\,-m\rangle\langle J\,k+k'|2\,2\,k\,k'\rangle \times d^{(J)}_{k+k'n}(\beta)d^{(J)}_{n0}(\theta)e^{i(k+k')\gamma}\rho_{2k}\rho_{2k'}. \qquad [23]$$

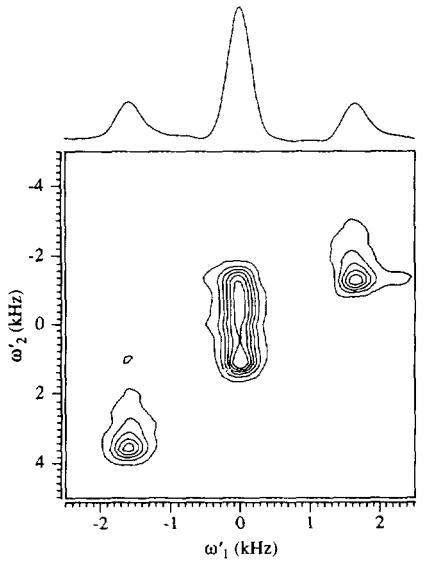

FIG. 9. Two-dimensional DAS spectrum of $^{207}PbNO_3$ using the $\theta_1 = 0°, \theta_1 = 90°$ angle pair, where $x_1 = 0.33$ and $x_2 = 0.67$. The rotor frequency was $\Omega_R = 1.2$ kHz. The projection onto the ω'_1 axis of the spectrum is devoid of first-order broadenings and contains spinning sidebands separated by integer multiples of $1.33\Omega_R = 1.6$ kHz.

In the DAS experiment the rotor angle θ is switched from θ_1 after the first evolution period t_1 to θ_2 for the second evolution period t_2. The phase of the magnetization in this experiment is given by

$$\Phi(t_1, t_2) = \int_0^{t_1} \Omega^{(2)}(\theta_1, t)dt + \int_{t_1}^{t_1+t_2} \Omega^{(2)}(\theta_2, t)dt$$

$$= W_0(\beta, \gamma, \theta_1)t_1 + W_0(\beta, \gamma, \theta_2)t_2$$

$$+ \sum_{n\neq 0} \frac{W_n(\beta, \gamma, \theta_1)}{n\Omega_R}[e^{in(\Omega_R t_1+\alpha)} - e^{in\alpha}]$$

$$+ \sum_{n\neq 0} \frac{W_n(\beta, \gamma, \theta_2)}{n\Omega_R}[e^{in(\Omega_R(t_1+t_2)+\alpha+\phi_R)} - e^{in(\Omega_R t_1+\alpha+\phi_R)}], \quad [24]$$

where ϕ_R is the relative phase of the rotor between the end of the first evolution period and the initiation of the second evolution period.

The signal $S(t_1, t_2)$ is then simply the exponentiation of this time-dependent phase. Using a property of delta functions (*26*) we obtain the following expression for $S(t_1, t_2)$,

$$e^{i\Phi(t_1,t_2)} = e^{iW_0(\beta,\gamma,\theta_1)t_1}e^{iW_0(\beta,\gamma,\theta_2)t_2}$$

$$\times \sum_{N_1=-\infty}^{\infty} \sum_{N_2=-\infty}^{\infty} \sum_{N_3=-\infty}^{\infty} \sum_{N_4=-\infty}^{\infty} A_{N_1}(\theta_1)A^*_{N_2}(\theta_1)A_{N_3}(\theta_2)A^*_{N_4}(\theta_2)$$

$$\times e^{-i[(N_1-N_2+N_3-N_4)\alpha+(N_1+N_3-N_4)\Omega_R t_1+N_3\Omega_R t_2+(N_3-N_4)\phi_R]}, \quad [25]$$

where

$$A_N(\theta) = \frac{1}{2\pi}\int_0^{2\pi} d\Theta \times \exp\left[iN\Theta + \sum_{n\neq 0} \frac{W_n(\beta, \gamma, \theta)}{n\Omega_R} e^{in\Theta}\right], \quad [26]$$

and $A^*_N(\theta)$ is the complex conjugate of $A_N(\theta)$.

From Eq. [25] it is not clear that the centerband and all sidebands will be real and positive. As mentioned earlier experimental and simulated 2D DAS spectra indicate that all sidebands of significant intensity are of the same phase. This can be analytically shown to be true if Eq. [25] is averaged over the powder angle α and one of the DAS angles is 0°. The average over α gives

$$\langle S(t_1, t_2)\rangle_\alpha = e^{iW_0(\beta,\gamma,\theta_1)t_1}e^{iW_0(\beta,\gamma,\theta_2)t_2} \times \sum_{N_1,N_2,N_3} A_{N_1}(\theta_1)A^*_{N_2}(\theta_1)A_{N_3}(\theta_2)A^*_{N_1-N_2+N_3}(\theta_2) \times e^{-i[N_2\Omega_R t_1+N_3\Omega_R t_2+(N_2-N_1)\phi_R]}. \quad [27]$$

When $\theta = 0°$ the amplitude $A_N(0°)$ will be zero except when $N = 0$, where $A_0(0°) = 1$. Thus for $\theta_1 = 0°$ we obtain $N_1 = N_2 = 0$ and

$$\langle S(t_1, t_2)\rangle_\alpha = e^{iW_0(\beta,\gamma,\theta_1)t_1}e^{iW_0(\beta,\gamma,\theta_2)t_2} \times \sum_{N_3} |A_{N_3}(\theta_2)|^2 e^{-iN_3\Omega_R t_2}, \quad [28]$$

and for $\theta_2 = 0°$ we obtain $N_3 = N_1 - N_2 = 0$ and

$$\langle S(t_1, t_2)\rangle_\alpha = e^{iW_0(\beta,\gamma,\theta_1)t_1}e^{iW_0(\beta,\gamma,\theta_2)t_2} \times \sum_{N_2} |A_{N_2}(\theta_1)|^2 e^{-iN_2\Omega_R t_1}, \quad [29]$$

In a similar fashion one can show that when θ_1 or θ_2 is 90°, all odd sidebands in the dimension associated with 90° are zero.

One approach that guarantees all sidebands to be real and positive for any rotor-angle pair is to average the signal over the rotor phase, ϕ_R, for each value of t_1 and t_2. By varying the rotor phase acquired during the hop, Eq. [25] can be averaged over ϕ_R, in addition to the powder angle α, to obtain $N_2 - N_1 = N_3 - N_4 = 0$ and

$$\langle S(t_1, t_2)\rangle_{\alpha,\phi_R} = e^{iW_0(\beta,\gamma,\theta_1)t_1} \sum_{N_1} |A_{N_1}(\theta_1)|^2 e^{-iN_1\Omega_R t_1} \times e^{iW_0(\beta,\gamma,\theta_2)t_2} \sum_{N_3} |A_{N_3}(\theta_2)|^2 e^{-iN_3\Omega_R t_2}. \quad [30]$$

ACKNOWLEDGMENTS

We thank Antoine Llor for helpful discussions. This investigation was supported by the Director, Office of Energy Research, Office of Basic Energy Sciences, Materials Sciences Division, and Office of Health and Environmental Research, Health Effects Research Division, of the U.S. Department of Energy under Contract DE-AC03-76SF00098. P.J.G. was supported by National Institutes of Health, National Research Service Awards, from the National Institute of General Medical Sciences. J.H.B. was supported by a National Science Foundation graduate fellowship.

REFERENCES

1. G. A. Williams and H. S. Gutowsky, *Phys. Rev.* **104,** 278 (1956).
2. E. R. Andrew, W. S. Hinshaw, and R. S. Tiffen, *J. Magn. Reson.* **15,** 191 (1974).
3. E. Lippmaa, M. Alla, and T. Tuherm, *in* "Magnetic Resonance and Related Phenomena: Proceedings of the XIXth Congress Ampere," p. 113, Groupment Ampere, Heidelberg, Sept. 1976.
4. M. M. Maricq and J. S. Waugh, *J. Chem. Phys.* **70,** 3300 (1979).
5. J. Schaefer and E. O. Stejskal, *J. Am. Chem. Soc.* **98,** 1031 (1976).
6. J. Herzfeld and A. E. Berger, *J. Chem. Phys.* **73,** 6021 (1980).
7. G. Bodenhausen, S. P. Kempsell, R. Freeman, and H. D. W. Hill, *J. Magn. Reson.* **35,** 337 (1979).
8. A. C. Kolbert, D. P. Raleigh, M. H. Levitt, and R. G. Griffin, *J. Chem. Phys.* **90,** 679 (1989).
9. A. Llor and J. Virlet, *Chem. Phys. Lett.* **152,** 248 (1988).
10. B. F. Chmelka, K. T. Mueller, A. Pines, J. Stebbins, Y. Wu, and J. W. Zwanziger, *Nature* **339,** 42 (1989).
11. K. T. Mueller, B. Q. Sun, G. C. Chingas, J. W. Zwanziger, T. Terao, and A. Pines, *J. Magn. Reson.* **86,** 470 (1990).
12. K. T. Mueller, G. C. Chingas, and A. Pines, *Rev. Sci. Instrum.* **62,** 1445 (1991).
13. P. J. Grandinetti, A. Llor, Y. K. Lee, J. H. Baltisberger, U. Werner, M. A. Eastman, and A. Pines, *J. Magn. Reson. A,* in press.
14. A. Samoson, E. Lippmaa, and A. Pines, *Mol. Phys.* **65,** 1013 (1988).
15. R. R. Ernst, G. Bodenhausen, and A. Wokaun, "Principles of Nuclear Magnetic Resonance in One and Two Dimensions," Oxford Univ. Press, Oxford, 1987.
16. K. Nagayama, P. Bachmann, K. Wüthrich, and R. R. Ernst, *J. Magn. Reson.* **31,** 133 (1978).
17. K. Nagayama, A. Kumar, K. Wüthrich, and R. R. Ernst, *J. Magn. Reson.* **40,** 321 (1980).
18. A. Bax, R. H. Griffey, and B. L. Hawkins, *J. Magn. Reson.* **55,** 301 (1983).
19. G. Wider, S. Macura, A. Kumar, R. R. Ernst, and K. Wüthrich, *J. Magn. Reson.* **56,** 207 (1984).
20. A. C. Kolbert, M. H. Levitt, and R. G. Griffin, *J. Magn. Reson.* **85,** 42 (1989).
21. G. Bodenhausen and R. R. Ernst, *J. Am. Chem. Soc.* **104,** 1304 (1982).
22. M. H. Levitt, *J. Magn. Reson.* **82,** 427 (1989).
23. W. T. Dixon, *J. Chem. Phys.* **77,** 1800 (1982).
24. D. P. Raleigh, E. T. Olejniczak, and R. G. Griffin, *J. Chem. Phys.* **89,** 1333 (1988).
25. M. Goldman, P. J. Grandinetti, A. Llor, Z. Olejniczak, and J. W. Zwanziger, *J. Chem. Phys.*, **97,** 8947 (1992).
26. M. Mehring, "Principles of High Resolution NMR in Solids," Springer-Verlag, Berlin/Heidelberg, 1976.